Chemico-Biological Interactions 405 (2025) 111303

Contents lists available at ScienceDirect

Chemico-Biological Interactions

journal homepage: www.elsevier.com/locate/chembioint

Research paper

Transcriptomic investigation of NP toxicity on HepaRG spheroids

Merve Erden Tüçer [a], Nazlıcan Tunç [a], Suat Tüçer [a], Rana Acar [b], Duygu Deniz Usta [c], Kouroush Salimi [d], Özlen Konu [a,b], Urartu Özgür Şafak Şeker [a,*]

[a] UNAM–Institute of Materials Science and Nanotechnology, National Nanotechnology Research Center, Bilkent University, 06800, Ankara, Turkey
[b] Bilkent University, Department of Molecular Biology and Genetics, 06800, Ankara, Turkey
[c] Gazi University, Faculty of Medicine, Department of Medical Biology and Genetics, 06500, Ankara, Turkey
[d] Ankara Yildirim Beyazit University, Faculty of Engineering and Natural Sciences, Department of Chemical Engineering, 06010, Ankara, Turkey

ARTICLE INFO

Keywords:
Nanoparticles
Transcriptomics
Nanotoxicity
Nanotechnology

ABSTRACT

Metal nanoparticles (NPs) are commonly used nanomaterials, however concerns have been raised about their toxicity. Although a few studies have reported the toxicity of NPs on cells, they have generally been restricted to a limited variety of NPs, inappropriate cell lines, or culture methods. Thus, the adverse effects remain inadequately understood, necessitating further analysis. This study focuses on assessing the impacts of diverse NPs of varying materials and sizes on HepaRG spheroids to determine the genes that respond to acute NP toxicity. HepaRG cells, the most appropriate alternative to primary hepatocytes, were cultured in 3D spheroids to better mimic the cellular microenvironment of the liver. To elucidate the toxicity mechanisms of NPs on HepaRG spheroids, transcriptome analysis was conducted by using RNA sequencing (RNA-seq). Among all NPs, lowest and highest numbers of differentially expressed genes (DEGs) were found for 40 nm AuNP (118 genes) and InP/ZnS (1904 genes), respectively. Remarkably, processes such as drug metabolism, sensitivity to metal ions, oxidative stress, endothelial-mesenchymal transition (EMT) and apoptosis consistently exhibited significant enrichment across all NPs of different materials. Pathways related to stress responses of the cells such as the MAPK, p53 and mTOR pathways are found to be dysregulated upon exposure to various NPs. The genes that are common and unique between DEGs of different NPs were identified. These results provide novel insights into the toxicological mechanisms of NPs on HepaRG spheroids.

1. Introduction

Nanotechnology has emerged as a prominent area of research, drawing attention since the last century. At the forefront of this field are NPs (NPs), the fundamental units of investigation. These materials generally constitute a vast category of matter up to 100 nm in size, differing in dimensions that include 0D, 1D, 2D, or 3D [1,2]. NPs possess unique properties due to large surface area, mechanical strength, optical activity, and chemical reactivity [3]. These distinctive properties of NPs have led to diverse applications in a wide array of fields, such as cosmetics, food and food packaging, drug delivery and medicine, bioremediation, paints, coatings, biosensing, and bioimaging [4,5]. Although NPs offer numerous advantages, they also have certain drawbacks. The high surface-to-volume ratio of NPs can cause cellular stress which consequently results in gene expression dysregulation, protein unfolding, DNA damage, and reactive oxygen species (ROS) production, leading to various health issues [6]. To assess the potential risk of injury to individuals exposed to NPs, it is important to understand the intrinsic toxicity of the substances [7]. To understand the potential hazards of NPs, we need further information about the mechanisms of their toxicity. Therefore, a thorough pathway analysis is essential to enhance our comprehension of the mechanisms of NP toxicity.

The liver is a pivotal organ for investigating the toxicity of NPs. Although most hepatic cell lines have a limited capacity for bioactivation, they can serve as an alternative to primary hepatocytes. The HepaRG cell line, on the other hand, is the first human cell line capable of in vitro differentiation into mature hepatocyte-like cells [8]. HepaRG cells are particularly attractive as a tool for studying differentiation, liver metabolism, metabolism and toxicity of drugs due to their progenitor nature, capacity to differentiate into biliary and hepatocyte phenotypes, and liver enzyme levels comparable to those of primary hepatocytes [9].

Toxicity tests modelled in two-dimensional (2D) cell cultures are overly simplistic, lack of tumor heterogeneity and cellular

* Corresponding author.
E-mail address: urartu@bilkent.edu.tr (U.Ö.Ş. Şeker).

https://doi.org/10.1016/j.cbi.2024.111303
Received 23 August 2024; Received in revised form 11 October 2024; Accepted 30 October 2024
Available online 6 November 2024

microenvironment [10]. The limitations inherent in 2D systems have prompted the evolution toward three-dimensional (3D) in vitro systems. To generate in vitro models that aptly replicate the intricacies of in vivo settings, the integration of 3D structures has emerged as a critical component that has previously been absent [11]. 3D cultures provide in vivo-like settings and facilitate essential cell-cell and cell-extracellular matrix (ECM) interactions that are essential for the regulation of cell behavior and function but are challenging to mimic in 2D [12]. 3D structures exhibit toxicity responses to external stimuli that are representative of those seen in vivo, owing to improved cell-cell and cell-ECM interactions [13]. For these reasons, we chose to use HepaRG spheroids as the toxicity testing model.

Toxicity testing lacks reliable and precise models. In the present research, we describe a model for toxicity testing that uses a hepatic cell line, HepaRG, which is the most similar model to primary hepatocytes. Additionally, the 3D culture of these cells increases the predictivity and precision of the results to in vivo studies. This study is novel in terms of using the HepaRG spheroids as a model for NP toxicity testing. NP toxicity is a concern that has arisen after the widespread use of them in diverse products. However, a detailed and comprehensive analysis of various NPs is missing. In this study, we analyze and compare the acute toxicity mechanism of eleven NPs of different materials and sizes. This is the first and most comprehensive study on NP toxicity on HepaRG cells because of comparing and interpreting eleven different NPs at the same time. Therefore, we employed four distinct types of NPs (namely AuNP, AgNP, TiO_2NP, and QDs) of varying sizes, in conjunction with HepaRG spheroids, to establish a system for monitoring NP cytotoxicity. We aimed to investigate the acute cytotoxicity of the NPs and find the genes that respond to stress conditions. Thus, the cells are exposed to NPs for 24 h. By conducting transcriptome analysis, we obtained detailed information about how HepaRG spheroids respond to cytotoxicity of various NPs, as well as identifying DEGs whose expressions were significantly altered. The genes that are shown to be dysregulated are considered as the forefront fight mechanism of the cells against NP toxicity. According to our results, NPs triggered the upregulation of the genes involved in metal ion homeostasis, apoptosis, EMT, ROS, and tumorigenesis pathways.

2. Materials and methods

2.1. Reagents

HepaRG cells (Cat.No. HPRGC10), Pen/Strep and FBS were purchased from Thermo Scientific. William's E Medium and hydrocortisone were purchased from Sigma Aldrich. Human insulin was purchased from pharmacy (Humulin N, 100U/mL).

2.2. Synthesis of Au, Ag, and TiO_2 NPs

The colloidal dispersions of gold NPs (AuNPs) were prepared using two different methods: the single-phase citrate stabilized Turkevich approach and two-phase Martin method [14,15]. In Martin method [14], a stock solution ("stock-A″) of 50 mM $HAuCl_4$ and 50 mM HCl was produced and stored at +7 °C in the dark. A second stock solution ("stock-B″) containing 50 mM sodium borohydride and 50 mM NaOH was prepared and kept at +7 °C. To make Au NPs (about 3 nm in size), 200 μL of stock-A with 20 mL of distilled water were mixed at room temperature. Next, 600 μL of stock-B solution was quickly added to the prepared solution and stirred for 5 min. The color of the final solution changed from light yellow to red. The Turkevich method [15] involves heating an aqueous solution containing $HAuCl_4$ (0.04 g in 48 mL DDI H_2O) to boiling while vigorously stirring. After 5 min of boiling, trisodium citrate (0.07 g) was added, and the process continued for 15 min. The colloidal Au NPs (~ 80 nm in size) were cooled to room temperature and kept in the dark for later use.

The colloidal solutions of AgNPs were synthesized according to the previously reported study with certain changes [16]. Typically, $AgNO_3$ (0.5 mM) was added into DDI water (100 mL) and the dispersion was stirred at room temperature for 10 min. Then, the as-prepared solution was heated to boiling and 1 mL of sodium citrate solution (1 % w/w) was added. The formation of Ag NPs was completed during the vigorous stirring for 1 h. The as-synthesized Ag NP solution was cooled to room temperature and kept in the dark for future use.

The colloidal dispersions of TiO_2NPs with size-controlled spherical morphologies were synthesized using a two-step core/shell technique [17,18]. Polydopamine NPs were initially synthesized as starting template by in-situ polymerization of dopamine hydrochloride. For this purpose, an aqueous solution containing ammonium hydroxide (7 mL), ethanol (20 mL), and DDI water (35 mL) were mixed at room temperature for 5 min. Then, dopamine hydrochloride aqueous solution (50 mg/mL) was immediately added into the as-prepared solution and agitated at room temperature for 16 h. PDA NPs were immediately collected via centrifugation-decantation method and washed with water and ethanol three times, respectively. A particular amount of ethanol (10 mL) was added to re-disperse PDA NPs (15 mg) under continuous stirring. Titanium isopropoxide (Ti(IP), 20 μL) was promptly added into the reaction medium and agitated for 1 h at room temperature. To finish the hydrolysis reaction, 500 μL of DDI water was added dropwise to the final reaction solution and mixed for 6 h. Finally, the size-controlled spherical TiO_2NPs were promptly collected and washed with ethanol and water using centrifugation-decantation. Characterization of NPs: NPs were characterized with TEM. 10uL of NPs were added on the TEM grid, and incubated 10 min. Then the NP solution was discarded, and the grids were washed with ddH_2O 2 times. Then left for drying for 10 min before analysis.

2.3. Cell culture

HepaRG cells were purchased from Thermo Scientific (Cat.No. HPRGC10). Cells were cultured in William's E Medium (Sigma Cat.No.: W1878) supplemented with 10 % FBS, 100 U/ml Pen/Strep, 2 mM L-glutamine, 32 mU/mL human insulin and 20 μg/mL hydrocortisone hemisuccinate. Cells were cultured in T25 flask until 80 % confluency changing medium every 2 days.

2.4. MTT assay

HepaRG cells that were cultured in T25 flask were collected with trypsin, then seeded into the 96 well plated in a density of 30,000 cells/well and cultured for 1 day. The other day, increasing concentrations of NPs were added on to the cells in fresh medium. Cells and NPs were incubated together for 24hr, and the medium was changed with 10 % MTT containing medium. After 4h of incubation, medium was discarded, and the purple crystals were dissolved in 100 μL DMSO. Measurements were taken with microplate reader at 560 nm.

2.5. Agarose method for spheroid formation

96 well plates were coated with 50 μL sterile 1.5 % cell culture grade agarose dissolved in PBS. Then HepaRG cells were seeded into the plate in a density of 3000 cells/well in 100 μL medium. Cells were cultured for 4 days for the spheroids to form. At day 4, the spheroids were collected and put into a 6 well plate coated with 2 mL 1.5 % agarose. Then the appropriate concentrations of NPs were added on to the spheroids, and incubated for 24 h. Next day, the spheroids were collected by centrifugation and were subjected to RNA isolation (M&N, NucleoSpin RNA, Cat.No.740955.50) procedure according to the manufacturer's protocol.

2.6. High-throughput transcriptomic sequencing

Total RNAs that are isolated from HepaRG spheroids (treated with gold NPs (3 nm, 15 nm, 80 nm), silver NPs (12 nm, 40 nm, 80 nm),

titanium NPs (25 nm, 100 nm, 300 nm) and 2 quantum dots for 24 h), (each NP and control group has 2 replicates). Total RNA was extracted using NucleoSpin (Macherey-Nagel™ NucleoSpin™ RNA, Mini Kit) following the manufacturer's protocol. The quantity and quality of RNA were examined by Termo ScientifcTM NanoDropTM 8000 Spectrophotometer. Library sequencing was performed on an Illumina Hiseq. 4000 platform, to create paired-end reads with a length of 150 bp.

2.7. Bioinformatics analysis

The quality control of RNA-Seq data was conducted using the FastQC with default parameters. The RNA-seq data was analyzed with Hisat2, StringTie and Ballgown. The analysis were done as it was described before [19]. Clean paired-end reads were aligned to the human reference genome sequence, GRCz10 version31, using Hisat2. The expression levels are calculated by StringTie. Differential expression analysis was done with Ballgown in R. The DEGs between two groups were selected based on the p-value<0.05 and |log2(fc)|>0.5. Volcano plots were plotted with ggplot package of R. To understand the functions of the differentially expressed genes, gene ontology (GO) and Hallmark gene set enrichment analysis were conducted with msigdbr package of R. KEGG pathway analysis was done with NIH DAVID Bioinformatics tool (https://david.ncifcrf.gov/tools.jsp). Heatmaps were plotted with ComplexHeatmap R package with the gene sets driven from GSEA gene lists.

2.8. Statistical analysis

The DEGs between two groups were selected based on the following criteria: 1) the p-value was less than 0.05 and 1) |log2 (fold change) |> 0.5. For GO enrichment analysis and KEGG pathway analysis P-value<0.05 was considered statistically significant.

3. Results

3.1. Characterization of NPs

To see the effects of the different sizes and materials on the NP properties on cells, we used 3 different materials of NPs of 3 different sizes of each which are gold (3 nm, 15 nm, 80 nm), silver (12 nm, 40 nm, 80 nm), titanium (100 nm, 300 nm and 500 nm) and we used 2 different quantum dots CdZnSe/CdZnS/ZnS (QD1) and InP/ZnS (QD2). The size and morphology of the NPs were characterized by transmission electron microscopy (TEM) (Fig. 1). Zeta potentials of the NPs were measured (Table S1).

3.2. Cell viability assays

For the differential gene expression analysis of the cytotoxicity of the NPs, we need to expose cells with toxic concentrations of NPs before RNA isolation. In this regard, we did cell viability assays to find the toxic concentrations of NPs of different materials and sizes on HepaRG cells. The viability of HepaRG cells exposed to varying concentrations of NPs were assessed by MTT assay. (Fig. 2). We decided to choose the toxic concentration of NPs which we collect mRNAs at is to be the concentration at which the viability is 80 %. We decided on this number, because we wanted the NP concentration to be toxic, however not too toxic to kill all the cells to enable mRNA isolation from these cells after NP exposure. As a result, the concentrations that resulted in 80 % viability are 20 μg/mL for 3 nm AuNP, 10 μg/mL for 15 nm AuNP, 10 μg/mL for 80 nm AuNP, 20 μg/mL for 12 nm AgNP, 50 μg/mL for 40 nm AgNP, 200 μg/mL for 80 nm AgNP, 20 μg/mL for 25 nm TiO_2NP, 10 μg/mL for 100 nm TiO_2NP, 10 μg/mL for 300 TiO_2NP, 20 μg/mL QD1 and 60 μg/mL QD2. Then we proceeded to collect the mRNAs after finding the toxic concentrations for each type and size of the NPs.

3.3. 3D spheroid culture

We used agarose-based spheroid culture method for the generation of spheroids. Compact and viable spheroids are formed. (Fig. 3A). It was previously reported that the spheroid diameter smaller than 300 μm prevents necrosis of the cells at the center [20]. For this reason we optimized the cell number accordingly, therefore, the diameter of the HepaRG spheroids is shown to be around 200 μm. Assessment of the viability of the cells inside the spheroid is done by staining the spheroids with Calcein-AM and propidium iodide (PI) dye. Both staining showed that the cells inside the spheroid are alive (Fig. 3B). Fixed spheroid staining was done as negative control. By the agarose coating method, the HepaRG spheroids were shown to be uniform and have the same sizes (Fig. S1A). Uniformity of the spheroids is ensured by culturing only one spheroid in one well of 96-well plate. Also, the viability of the HepaRG cells in the spheroid is ensured by optimizing the size of the spheroid which is around 200 μm. On day 6 of culturing, the spheroids are shown to be viable (Fig. S1B).

3.4. Transcriptome assembly and differential expression analysis

RNA-seq raw data was analyzed by using Hisat, and read counts were calculated by feature counts. RNA-Seq transcriptome was performed and approximately 20 million 150 bp sequence reads were obtained from each sequencing run from which more than 90 % were uniquely mapped into the human genome (Table S2). About 47–52 % of GC content was observed among the sequencing reads.

Transcriptomic analysis provided detailed information on how HepaRG cells respond to NP cytotoxicity and which genes significantly changed their expression. For the proceeding analysis, we set the criteria of $p < 0.05$ and $|log2FC| > 0.5$ for the determination of the DEGs. Volcano plots were generated to display the changes in the gene expression profiles of HepaRG cells upon NP treatment (Fig. 4A). According to the results, 3 nm, 15 nm and 80 nm AuNP treated cells have 370 (157 down and 213 upregulated), 116 (48 down and 68 upregulated), 205 (83 down and 122 upregulated) DEGs, respectively. In silver group, 12 nm, 40 nm and 80 nm AgNPs have 178 (60 down and 118 upregulated), 977 (517 down and 460 upregulated) and 711 (432 down and 279 upregulated) DEGs, respectively. Also, 25 nm, 100 nm and 300 nm TiO2NPs have 538 (359 down and 179 upregulated), 366 (148 down and 218 upregulated), and 660 (373 down 287 upregulated) DEGs, respectively. Lastly, QD1 and QD2 have 692 (378 down and 314 upregulated) and 1904 (1093 down and 811 upregulated) DEGs, respectively. The top 10 upregulated and downregulated genes were shown in for each NP (Fig. S2). There are common and unique genes between different sizes and materials of NPs. The number of common and unique DEGs among NPs were shown in Venn diagrams (Fig. 4B).

Combined DEGs for each material of NPs has given the 5 common genes that were enriched in all four materials of NPs, which are described in Table 1. Functions of these genes are related to tumor promotion, inflammation and EMT.

3.5. Functional analysis of DEGs

In genome wide expression studies, many DEGs are found by data analysis, and they need to be categorized to relate them to pathways or biological processes. To determine the function of DEGs and metabolic pathway enrichment, DEGs were subjected to gene set enrichment analysis. Top 10 enriched hallmark gene sets are shown (Fig. 5). Many upregulated genes showed enrichment in similar pathways among NPs that are related to heme metabolism, EMT, stress responses, tumor suppressor pathways, inflammatory and antioxidant pathways, and apoptosis. The DEGs were also analyzed by Gene Ontology gene sets (Fig. S3). The top enriched pathways are ribose phosphate biosynthetic process (GO:0046390) for 3 nm AuNP, mitochondrial DNA metabolic process (GO:1901858) for 15 nm AuNP, positive regulation of lipid

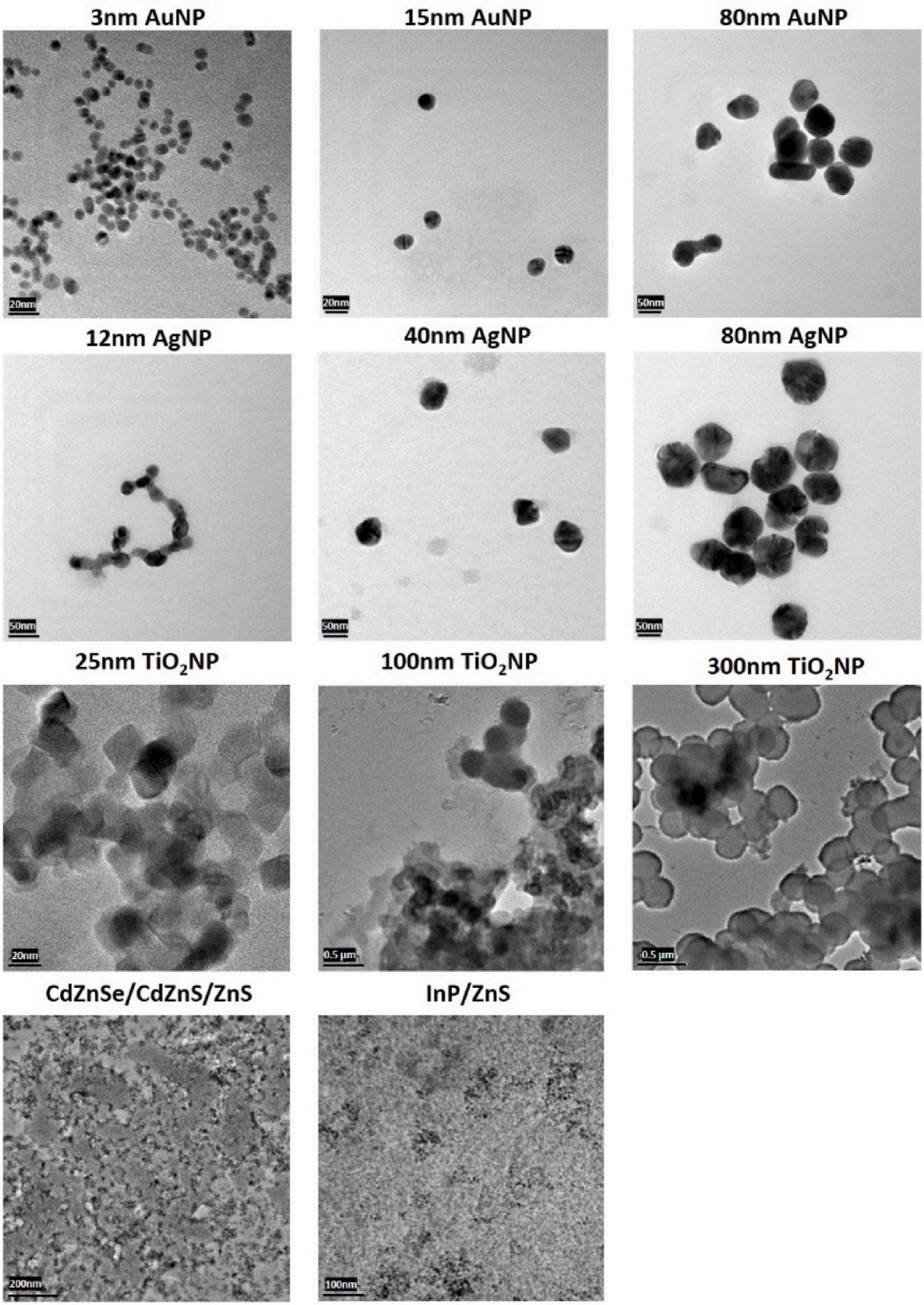

Fig. 1. Characterization of NPs with TEM.

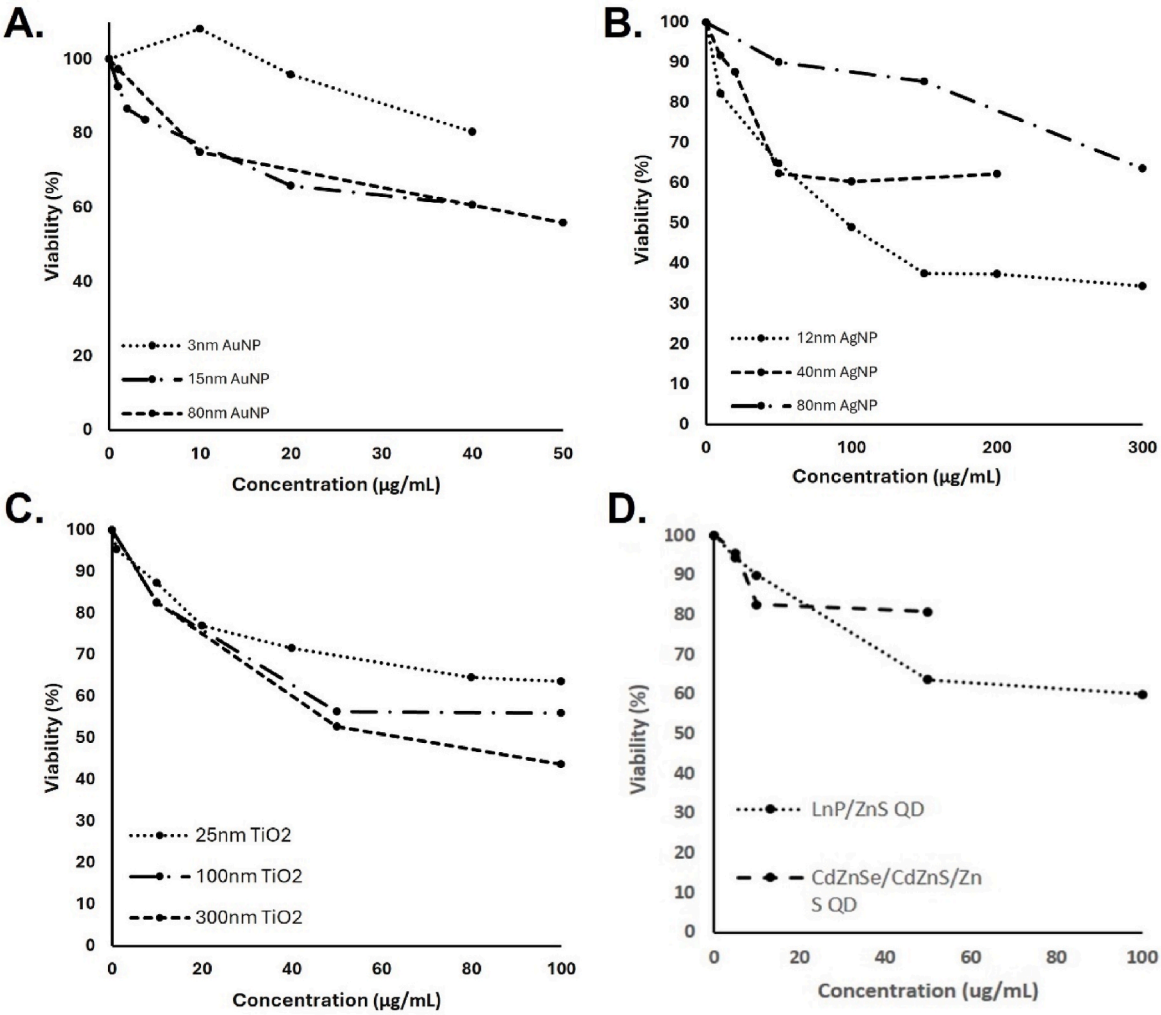

Fig. 2. Cytotoxicity of NPs on HepaRG cells for 24 h. Cytotoxicity of **A)** Gold NPs (3 nm, 15 nm, and 80 nm) and **B)** Silver NPs (12 nm, 40 nm, 80 nm) **C)** Titanium NPs (25 nm, 100 nm and 300 nm) and **C)** QDs (LnP/ZnS, CdZnSe/CdZnS/ZnS). Each value represents the mean ± SE of 3 repeats (N = 3).

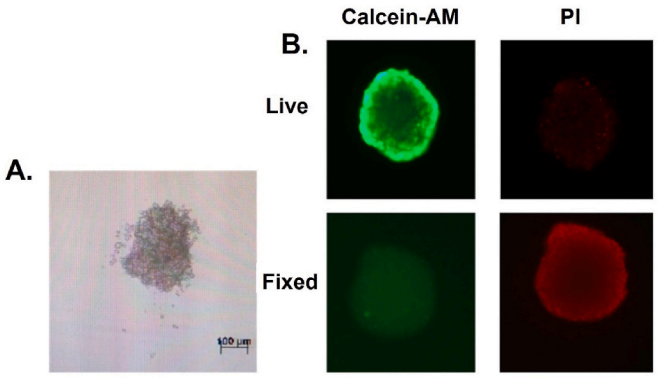

Fig. 3. Visualization and viability assessment of 3D spheroids of HepaRG cells. **A)** Bright-field microscopy image of HepaRG spheroids. **B)** The viability of the spheroid is tested with Calcein-AM and PI. Then, another spheroid was fixed with 70 % ethanol for 10 min and staining was done with Calcein-AM and PI as control for the viability.

catabolic process (GO:0050996) for 80 nm AuNP, positive regulation of mitotic cell cycle (GO:0045931) for 12 nm AgNP, urea metabolic process (GO:0019627) for 40 nm AgNP, sulphur compound metabolic process (GO:0006790) for 80 nm AgNP, cellular amino acid metabolic process (GO:0006521) for 25 nm TiO_2NP, regulation of cell-cell adhesion mediated by cadherin (GO:2000047) for 100 nm TiO_2NP, negative regulation of B cell apoptotic process (GO:0002903) for 300 nm TiO_2NP, cellular component assembly involved in morphogenesis (GO:0010927) for QD1 and alcohol metabolic process (GO:0006066) for QD2. Although many of the NPs have enriched similar pathways, the genes that activated these pathways were not mostly common.

To find the pathways that the DEGs were involved in, Kyoto Encyclopedia of Genes and Genomes (KEGG) pathway analysis was carried out with the DEGs of each NP. In most of the NPs, we observe pathways related to various diseases and disorders including hepatitis, rheumatoid arthritis, cancer, Parkinson, Huntington (Table 2).

3.6. Liver specific genes

Human cytochrome P450 (CYP) enzymes functions in the detoxification of drugs, cellular metabolism and homeostasis and they are mainly expressed in the liver [28,29]. These enzymes oxidize drugs that would be toxic, to eliminate them from the body. There are more than 50 CYP450 enzymes, but the isoforms of CYP1, 2, and 3 family enzymes are responsible with the metabolism of the drugs, especially CYP1A2, CYP2C9, CYP2C19, CYP2D6, CYP3A4, and CYP3A5 enzymes metabolize 90 percent of drugs [30]. Differential expressions of many CYP450 enzymes were observed in the NP exposed cells (Fig. 6A).

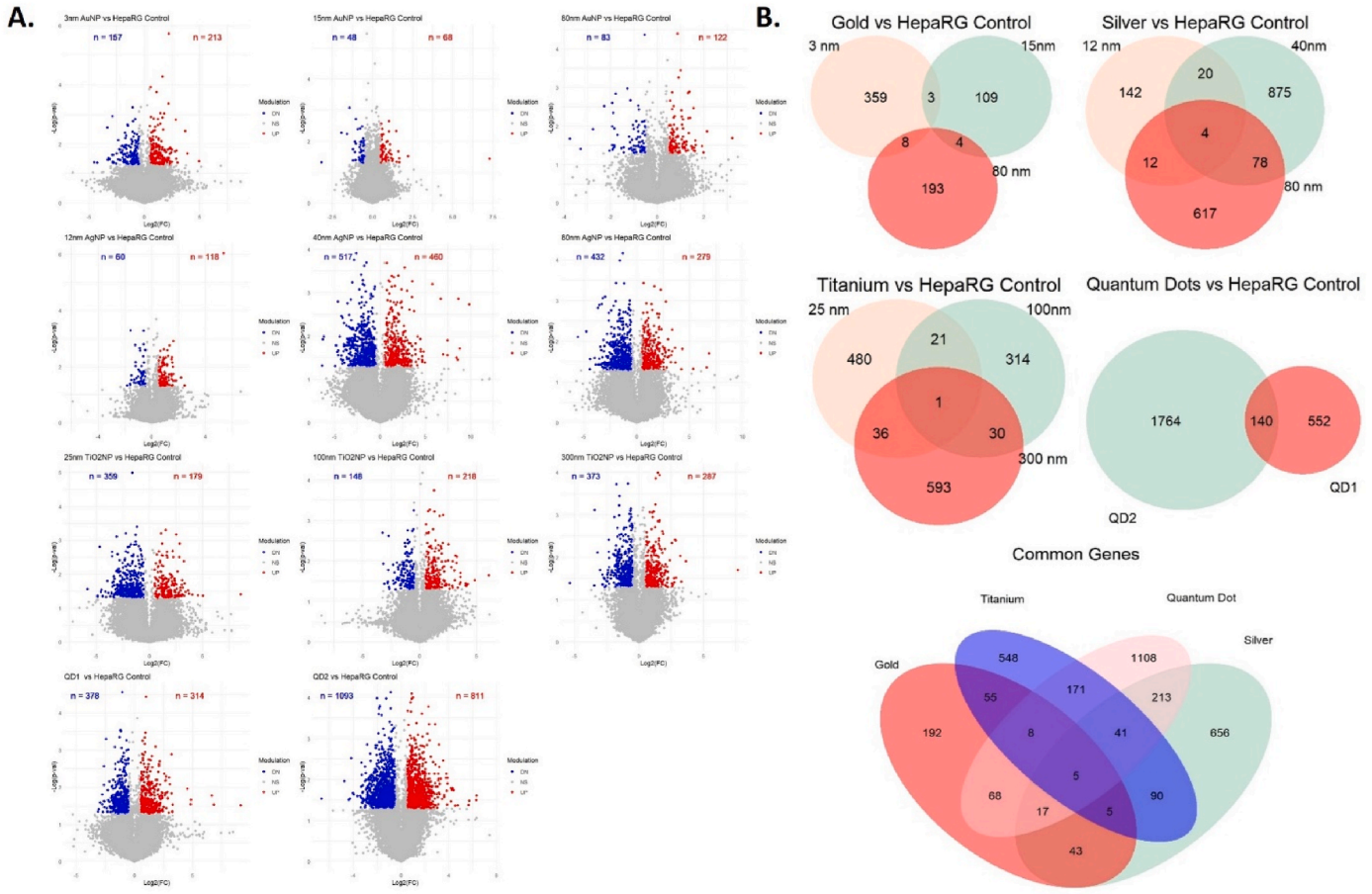

Fig. 4. Changes in the gene expression profiles of the cells exposed to each NP. **A)** Volcano plots of gene expression profiles of the HepaRG cells exposed to each NP. Upregulated DEGs (red), downregulated DEGs (blue) and non-significant genes (grey). **B)** Venn diagrams showing the number of DEGs in each transcriptome produced in response to each NP and common DEGs among the same materials of NPs.

Table 1
Common genes among NPs were shown with their fold change and function.

Gene Name	Gold FC	Silver FC	Titanium FC	QD FC	Function
IMPA2	2.16	2.37	2.87	2.13	Oncogene [21,22]
AC078850.1	1.88	3.26	4.61	4.60	Pyroptosis, Inflammation [23]
OPN3	1.42	1.71	2.52	1.63	Epithelial-Mesenchymal Transition and Metastasis [24]
HS3ST3B1	2.82	2.89	4.64	3.89	Epithelial-Mesenchymal Transition [25,26]
NUP85	1.44	1.75	1.55	3.00	Inflammation, liver disease [27]

3.7. Metal ion response genes

Solute Carrier proteins (SLC) are membrane-bound transporters that are involved in the uptake of the compounds into the cells. Their inhibition is related to drug resistance in some diseases, meaning that the drugs are transported via these transporters [31]. Overexpression of the metal ion SLC transporters are observed in NP exposed cells (Fig. 6B). AuNPs have the least to induce the expression of the SLC transporters, while other NPs induce the overexpression of at least 2 genes of this family. Once the NPs are in the cell, cellular response to metal ions is mostly regulated by the metallothionein family of genes (Fig. 6C). They act as antioxidants and they play a role in the detoxification of heavy metals [32]. All NPs, except 3 nm AuNP, induced the expression of at least one metallothionein.

3.8. Oxidative stress response genes

As reported earlier, NPs release ions inside the cells, and these ions react with other compounds resulting in the production of reactive oxygen species (ROS) [33]. Increased levels of ROS in the cell induces the expression of antioxidants to eliminate the ROS, because excessive production of ROS causes oxidative stress leading to DNA damage or dysfunction of various organelles. When ROS levels are elevated in the cells, some antioxidant enzymes are activated which means that cells have auto control defend mechanism against excessive ROS. As reported, TXN gene encodes a redox protein called thioredoxin which functions as an antioxidant enzyme. Also, ATOX1 functions in the antioxidant defense mechanism. It transports copper which is crucial for the antioxidant enzymes [34]. In response to the stress induced by exposure to NPs, HepaRG cells showed elevated levels of the antioxidant genes ATOX1, TXN, PTPA (Fig. 6D). These proteins manage the ROS elimination that are known to arise during oxidative stress and other stress conditions.

3.9. Apoptotic genes were enriched in all NPs

NPs cause apoptosis on cells [35,36]. NP treatment induced apoptotic gene expression in HepaRG cells. Apoptotic genes CD14, APP, TOP2A, DCN, IGFBP6, TIMP2, MMP2, F2R CCND1 genes were upregulated in response to NP toxicity (Fig. 6E). These data illustrated the high

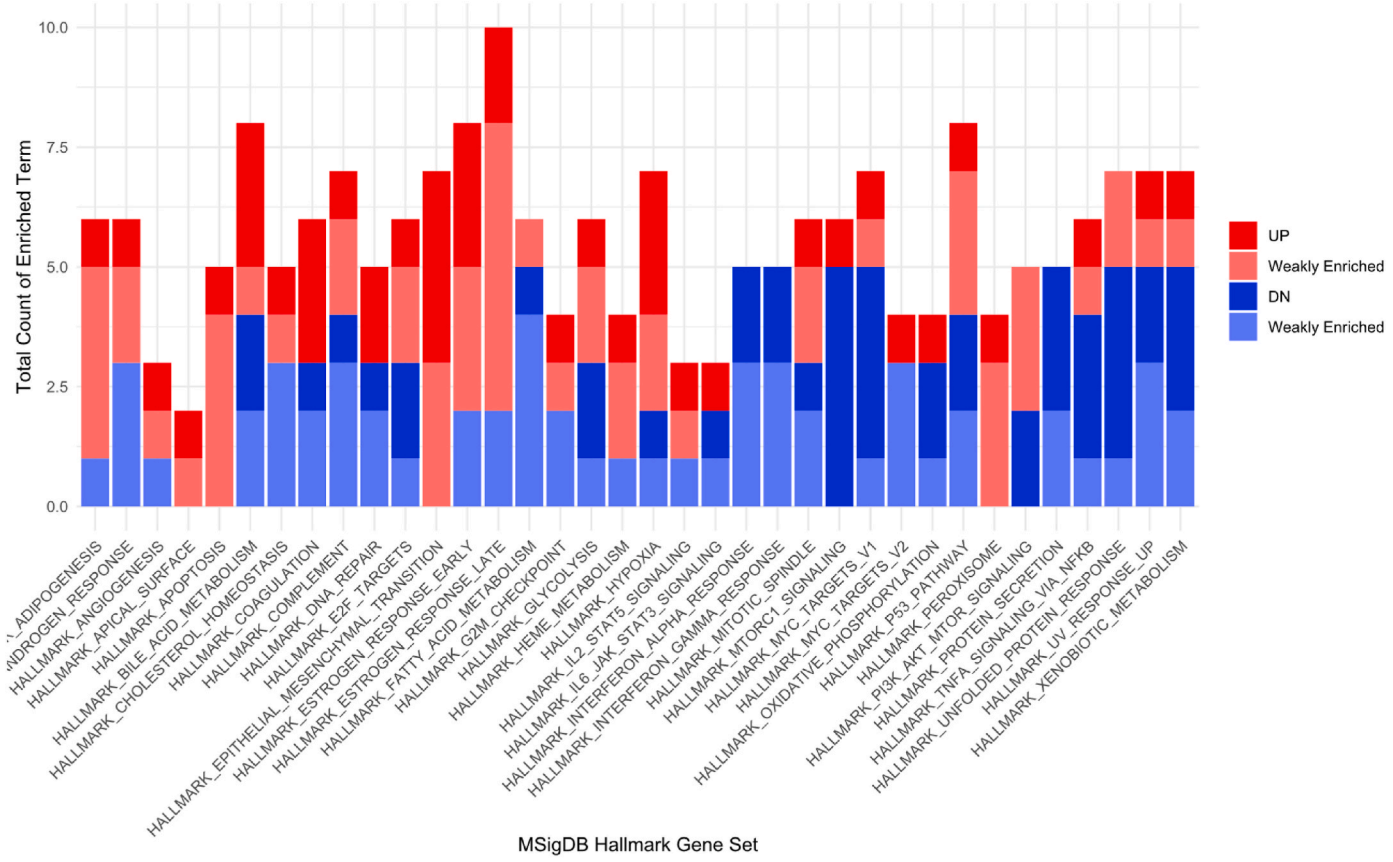

Fig. 5. Hallmark gene set enrichment analysis of DEGs.

toxicity potential of the NPs were common for all material and size of the NPs.

3.10. Metastasis and carcinogenic effect of NPs

In NP exposed cells, EMT marker genes were found to be differentially expressed (Fig. 6F). ANLN and MMP2 were upregulated in all the NPs. EDNRB were upregulated in gold, silver and titanium, however not upregulated in QD. This shows the different mechanisms of toxicity between different materials of NPs. Also, genes related to liver cancer were differentially expressed in all types of NPs (Fig. 6G).

4. Discussion

The present study performed a transcriptomic analysis on HepaRG spheroids exposed to several sizes and materials of NPs. HepaRG cells are of great importance in the toxicity and drug metabolism testing experiments since they have the most similar P450 enzymatic activities and drug metabolizing proteins to the primary liver cells [37]. Also, by culturing those cells in 3D spheroid form, we aimed to mimic the microenvironment of the cells in the liver. It was previously shown that in 3D culture HepaRG cells are a good model for in vitro genotoxicity testing since they retain their CYP enzyme activities even higher activity of some enzymes than 2D cultured cells [38]. HepaRG spheroids are the alternative for in vivo experiments. Here we showed that HepaRG spheroids can improve predictivity and precision of in vitro models for detecting toxic agents.

Considering the literature about NP toxicity, this is the first study that reveals the toxicity responses of HepaRG spheroids against 11 different NPs. Toxicity response is well known for other cells, however, the response of HepaRG cells to stress conditions needed to be investigated. In this study, our results revealed that HepaRG cells have both common and distinct responses to each different material and size of the NPs, thus they changed their transcriptome accordingly.

NPs were shown to cause cytotoxicity on cells [39]. Upon exposure to different NPs, HepaRG cells changed the regulation of many genes. They upregulated the expression of 5 genes common among all materials of NPs. These genes are IMPA2, AC078850.1, OPN3, HS3ST3B1 and NUP85, which are all upregulated. The functions of these genes are related to tumor-promoting, cell death, inflammation, liver disease and EMT. This means exposure to NPs caused significant cytological damage and carcinogenic effect on HepaRG cells.

Hallmark gene set analysis showed enrichment of the differentially expressed genes (DEGs) in apoptosis, estrogen response, heme metabolism, EMT, hypoxia, p53 pathway, coagulation and peroxisome. Exposure to toxic agents increases excessive ROS production in the cells. Excess ROS molecules cause oxidative stress by disrupting redox homeostasis in the cells that may result in many biological processes, such as protein damage, organelle damage, DNA damage, inflammatory response. Oxidative stress is an important factor that might promote cell death in response to NP toxicity. Increased expression of ROS pathway associated genes suggests the presence of oxidative stress upon NP treatment. ATOX1, TXN, PTPA overexpression reveals that the cells activated the ROS eliminating antioxidants. They function for cellular metal balance, scavenging ROS, and cellular responses to stress. When the cells cannot eliminate excess ROS, free radicals may attack membranes of the cell and organelles which cause activation of EMT causing genes. In the hallmark gene set enrichment analysis, we identified overexpression of MMP family proteins which are called metalloproteinases. They are associated with many signaling pathways including EMT, p53 and mTOR and their expressions are dysregulated in many cancer types [40,41]. Apoptosis and p53 pathways were considered because of the NP damage to the cells. Apoptotic genes CD14, APP, TOP2A, DCN, IGFBP6, TIMP2, MMP2, F2R, CCND1 were differentially

Table 2
KEGG pathways that are significantly enriched in DEGs.

NP	Term	Count	Pathway ID	PValue
3 nm AUNP	Ferroptosis	4	hsa04216	1.109E-02
	Ubiquitin mediated proteolysis	6	hsa04120	2.056E-02
15 nm AUNP	Metabolic pathways	12	hsa01100	2.891E-03
	Tyrosine metabolism	3	hsa00350	4.928E-03
80 nm AUNP	Complement and coagulation cascades	4	hsa04610	1.334E-02
	Fatty acid degradation	3	hsa00071	2.443E-02
	Type II diabetes mellitus	3	hsa04930	2.883E-02
	Pyruvate metabolism	3	hsa00620	2.883E-02
	Coronavirus disease - COVID-19	5	hsa05171	4.496E-02
12 nm AGNP	Fanconi anemia pathway	4	hsa03460	2.863E-03
	Cell cycle	5	hsa04110	8.950E-03
	Human T-cell leukemia virus 1 infection	5	hsa05166	2.815E-02
40 nm AGNP	Biosynthesis of amino acids	9	hsa01230	2.099E-03
	Biosynthesis of cofactors	13	hsa01240	2.719E-03
	Aminoacyl-tRNA biosynthesis	8	hsa00970	4.074E-03
	Vibrio cholerae infection	7	hsa05110	4.605E-03
	Epithelial cell signaling in Helicobacter pylori infection	8	hsa05120	6.108E-03
	Metabolic pathways	65	hsa01100	8.331E-03
	Rheumatoid arthritis	9	hsa05323	8.390E-03
	Collecting duct acid secretion	5	hsa04966	1.016E-02
	Glycolysis/Gluconeogenesis	7	hsa00010	1.697E-02
	Amyotrophic lateral sclerosis	20	hsa05014	2.097E-02
80 nm AGNP	Protein processing in endoplasmic reticulum	11	hsa04141	1.824E-03
	Nucleocytoplasmic transport	7	hsa03013	1.910E-02
	Human T-cell leukemia virus 1 infection	10	hsa05166	3.094E-02
	Hepatitis C	8	hsa05160	3.648E-02
	Acute myeloid leukemia	5	hsa05221	4.385E-02
	Autophagy - animal	8	hsa04140	4.807E-02
25 nm TiO_2NP	Protein processing in endoplasmic reticulum	15	hsa04141	3.207E-06
	Thyroid cancer	5	hsa05216	4.784E-03
	Glioma	6	hsa05214	1.358E-02
	Epstein-Barr virus infection	10	hsa05169	1.369E-02
	Viral carcinogenesis	10	hsa05203	1.452E-02
	Nucleocytoplasmic transport	7	hsa03013	1.547E-02
	Human T-cell leukemia virus 1 infection	10	hsa05166	2.372E-02
	Endometrial cancer	5	hsa05213	2.406E-02
	Longevity regulating pathway	6	hsa04211	2.629E-02
	Hepatitis C	8	hsa05160	2.903E-02
100 nm TiO_2NP	EGFR tyrosine kinase inhibitor resistance	4	hsa01521	4.526E-02
	Fluid shear stress and atherosclerosis	5	hsa05418	4.178E-02
	Ubiquitin mediated proteolysis	5	hsa04120	4.289E-02
	MAPK signaling pathway	7	hsa04010	4.807E-02
300 nm TiO_2NP	Glycine, serine and threonine metabolism	6	hsa00260	7.203E-04
	Metabolic pathways	44	hsa01100	1.309E-03
	Carbon metabolism	7	hsa01200	1.659E-02
	p53 signaling pathway	5	hsa04115	4.322E-02
	RNA degradation	5	hsa03018	4.874E-02
QD1	Alzheimer disease	22	hsa05010	2.610E-04
	Pathways of neurodegeneration - multiple diseases	24	hsa05022	7.355E-04
	Oxidative phosphorylation	11	hsa00190	1.306E-03
	Parkinson disease	16	hsa05012	1.491E-03
	Prion disease	16	hsa05020	1.917E-03
	Amyotrophic lateral sclerosis	19	hsa05014	2.285E-03
	Butanoate metabolism	5	hsa00650	3.187E-03
	Valine, leucine and isoleucine degradation	6	hsa00280	4.767E-03
	Huntington disease	16	hsa05016	5.519E-03
	mTOR signaling pathway	9	hsa04150	2.978E-02
QD2	Protein processing in endoplasmic reticulum	32	hsa04141	2.022E-07
	Aminoacyl-tRNA biosynthesis	18	hsa00970	8.854E-07
	Selenocompound metabolism	8	hsa00450	5.939E-05
	Protein export	10	hsa03060	1.267E-04
	AMPK signaling pathway	21	hsa04152	1.409E-04
	mTOR signaling pathway	23	hsa04150	7.226E-04
	Human T-cell leukemia virus 1 infection	29	hsa05166	7.994E-04
	Proteasome	10	hsa03050	2.833E-03
	Prion disease	31	hsa05020	5.583E-03
	Longevity regulating pathway	14	hsa04211	6.192E-03

expressed. The mechanism that NP toxicity may cause apoptosis is through ROS production. Excessive ROS may cause lipid peroxidation, mitochondrial damage or DNA damage that might consequently lead the cells to apoptosis [42]. Our results revealed that NPs cause excessive ROS production and consequently activate the genes related to EMT, apoptosis, coagulation and peroxisomes. Heme metabolism was enriched because metal ion response and metal transporters were enriched upon NP treatment by the genes GCLM, HBB, and ENDOD1. Metal transporters are responsible for the uptake of the NPs and metal ion response genes are responsible for the detoxification of these

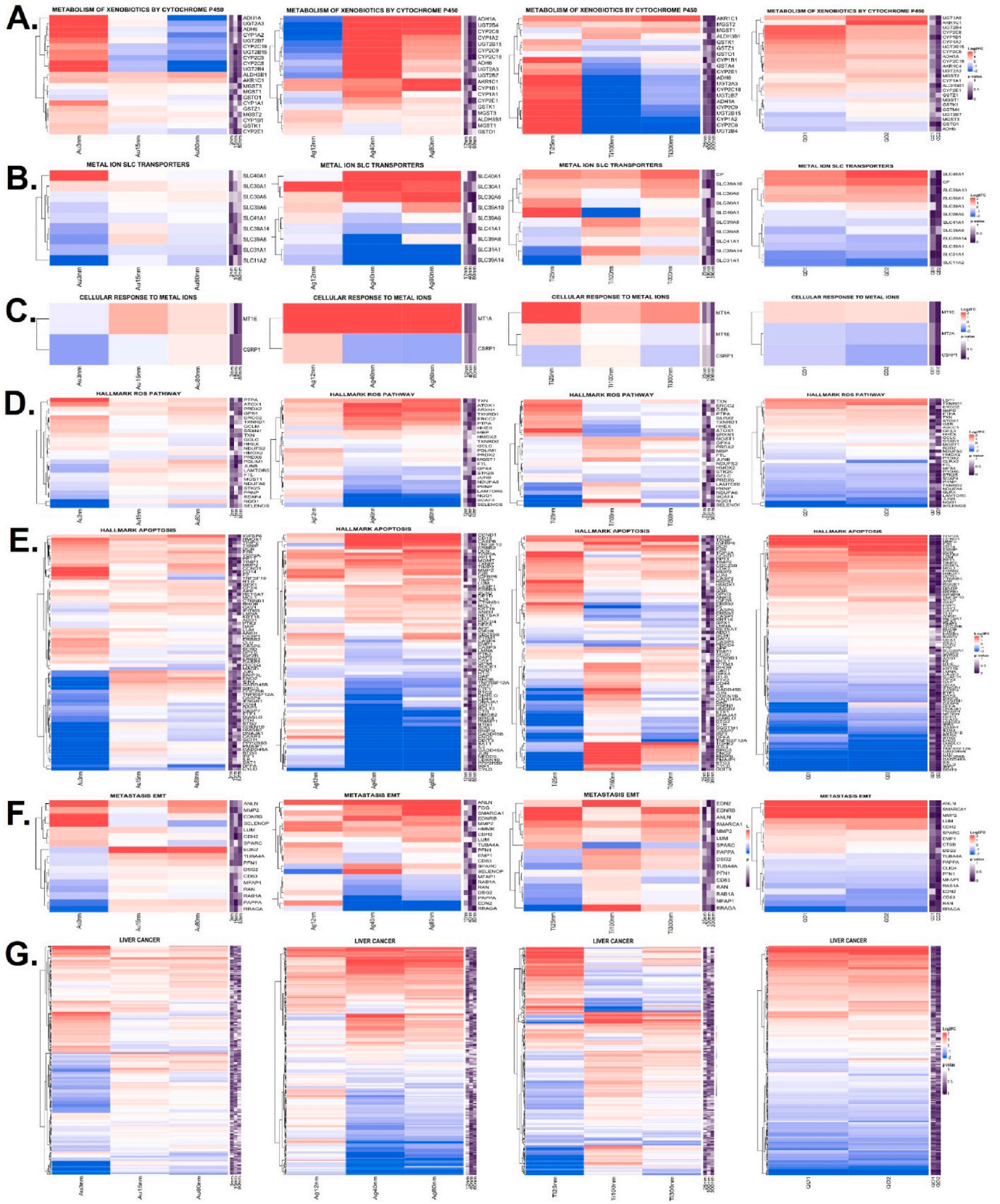

Fig. 6. Heatmaps of the gene sets that belong to specific pathways. Heatmaps of the **A)** Cytochrome P450 genes **B)** Metal ion transporter genes **C)** Metal ion response genes **D)** Metastasis genes **E)** ROS pathway genes **F)** Apoptosis genes **G)** Liver cancer related genes.

particles. NPs have endocrine disruptive effects and causes oxidative stress [43]. This phenomenon might be the reason of the overexpression of estrogen response in the cells. It is known that ROS causes coagulation and peroxisomes were activated as a response to increased ROS levels in the body [44]. ROS is accumulated in peroxisomes inducing the activation of antioxidant enzymes. Peroxisomes are the cellular location of many antioxidant enzymes. They are the important mediators of oxidative stress and regulators of oxidative stress-related signaling pathways. They have an important role in redox homeostasis [45,46]. Gene ontology analysis showed enrichment of the DEGs in DNA synthesis related pathways. Genotoxic effects of NPs are well known [47]. DNA damage may cause apoptosis or cell cycle arrest. Activation of DNA synthesis might indicate DNA damage caused by the NPs [48]. Also, lipid metabolism and membrane depolarization genes were upregulated, which reminds us the capability of NPs to disrupt cell membrane [49]. Treatment with metal NPs, the cells are exposed to metal ions since theories suggest that the NPs release metal ions that disrupt cation homeostasis in cells, leading to cellular damage [33,50]. So, the activation of pathways related to metal ion response is not surprising and shows that the cells are responding to these metal ions. These results indicate that the cells are exposed to the metal ions when treated with NPs, and these metal ions are activating the pathways that function for the cellular metal ion homeostasis.

NPs induce intracellular ROS production because of their strong oxidation ability [51]. Excess ROS production results in damage in DNA, organelles, cell membrane and cause lipid peroxidation and apoptosis [52]. The cells must sustain the balance between the ROS production and antioxidant defense mechanism to survive. Cells have enzymatic and non-enzymatic antioxidants that retain the redox balance [53]. Cellular antioxidant defense system eliminates excess ROS from the cells by converting them to non-toxic substances. This mechanism ensures the protection of cells from oxidative stress. Increased ROS production causes cells to activate detoxification pathways [54]. This involves activation of antioxidant genes which are the scavengers of ROS to prevent any damage to the cells. Upregulation of antioxidant genes such as ATOX1, TXN, PTPA in the HepaRG cells indicates the high levels of ROS production in the cells. An imbalance between the ROS production and antioxidants causes disruption of the redox homeostasis. NPs may cause very high levels of ROS production which may cause oxidative stress. Consequently, NPs may have led the cells to toxicity through oxidative stress caused by ROS production. Increased production of ROS is strongly associated with inflammation. TNF-alpha pathway activation and interleukin production indicates inflammation in the HepaRG cells after NP exposure.

The small size of the NPs enables them to penetrate into the cells and interact with molecules in the cells causing oxidative stress, DNA damage and inflammation [55]. Carcinogenic potential of the NPs was reported previously in many studies because of their genotoxic effects on cells [56–58]. The mechanism that NPs might induce the cells to evolve to tumor cells is the ability to cause DNA damage. In our results, we found that NP exposure induced the expression of epithelial to mesenchymal transition genes (MMP14, ITGB5, TIMP1, MMP2) and the genes that are related to liver cancer. Enrichment of pathways related to several types of cancer reveals the carcinogenic capability of NPs.

Employing eleven different NPs with varying materials and sizes necessitates interpreting the parameters. In terms of number of DEGs, the biggest change in the expression profile was observed in NPQD2, and the second one was the 40 nm AgNP. We saw that there is no relation between the material/size of the NPs on the number of the DEGs. However, we observed a relation between the number of DEGs and the heatmaps of the stress related pathways. As 3 nm AuNP had the highest number of DEGs among gold NPs, it had a different pattern than the other 2 gold NPs in the heatmaps. We can see that 15 nm and 80 nm AuNP had similar heatmap for stress related genes, whereas 3 nm AuNP was different than these two. A similar scenario applies for the silver NPs. 12 nm AgNP had a low number of DEGs whereas other two NPs had relatively high numbers of DEGs, and they also had similar pattern of heatmaps which is different than 12 nm AgNP. In quantum dots, both NPs had similar patterns in heatmaps despite having a huge difference in the number of DEGs. In the case of titanium NPs, there is not a stable pattern of heatmaps nor a relation between the DEGs and the heatmaps. These findings may show that the sizes of the nanoparticles change the potential of toxicity of NPs which eventually changes the number of DEGs. Cells that are exposed to higher toxicity changed their expression profiles more. The most common pathways that were activated upon toxicity of NPs of differing sizes and materials are related to the metabolism of proteins, fatty acids or nucleic acids. Especially, amino acid metabolism was observed in all the nanoparticles which may show that there are high levels of protein synthesis and degradation to ensure the expression of stress related genes. Also, some NPs induced the expression of the genes related to some diseases. In terms of gold NPs, only 80 nm AuNP induced the expression of disease related genes such as diabetes and COVID-19. Many pathways including anemia and infection were activated by all sizes of silver NPs. Moreover, all sizes of TiO2NP enriched pathways related to cancer. Upregulation of EGFR, MAPK and p53 are associated to cancer progression or inhibition [59–61]. Interestingly, both QDs induced the expression of mTOR pathway which is related to cancer progression [62]. The results show that in general different processes were activated upon exposure to different NPs, which may be the result of the reactivity of nanoparticle toxicity that is affected by the size, charge, shape, material etc.

The common impacts of NPs include oxidative stress, apoptosis, EMT and carcinogenesis. The distinct impacts are related to the physicochemical properties of NPs which change their biological activities and their interaction with the cells and other compounds. Their different behaviors and effects are due to different factors such as particle size, surface, composition, metal release type. These factors affect the interaction of these NPs with the cells and cellular compounds, which in turn change the mechanism of toxicity. With different properties, they cause different expression profiles in HepaRG cells. Although they enrich similar pathways and terms, they generally do this by upregulating different genes that belong to the same pathway. This means although their toxicity on HepaRG cells is common, the way that they expose them is different for each size and material.

5. Conclusions

In summary, our study showed that differing sizes and materials of NPs cause cytotoxicity and activate the pathways related to stress response in HepaRG cells. The size and material type changes the mechanism of cytotoxicity and expresses different genes, however all in all their impact on cells are mostly common. The genes that we indicated in this study belong to the response mechanism of HepaRG cells against NP toxicity. Biosafety assessment of nanoparticles lacks reliable and precise models. Our future studies will be focused on whole cell biosensor circuit design by using the promoter regions of the differentially expressed genes indicated in this study coupled with a reporter protein (such as GFP) to detect the toxicity of NPs and other compounds (drugs, chemicals) in various resources. This biosensor may improve future development of biosafety assessment systems as an alternative to animal tests with high predictivity of in vivo.

CRediT authorship contribution statement

Merve Erden Tüçer: Writing – review & editing, Writing – original draft, Investigation, Formal analysis, Conceptualization. **Nazlıcan Tunç:** Formal analysis, Data curation. **Suat Tüçer:** Formal analysis, Data curation. **Rana Acar:** Methodology, Formal analysis, Data curation. **Duygu Deniz Usta:** Methodology. **Kouroush Salimi:** Methodology, Investigation. **Özlen Konu:** Formal analysis, Data curation, Conceptualization. **Urartu Özgür Şafak Şeker:** Writing – review & editing, Writing – original draft, Supervision, Project administration,

Investigation, Funding acquisition, Formal analysis, Conceptualization.

Data statement

The data underlying this article are available in Zenodo repository at https://dx.doi.org/10.5281/zenodo.10451061 and https://dx.doi.org/10.5281/zenodo.10461091.

Declaration of competing interest

The authors declare the following financial interests/personal relationships which may be considered as potential competing interests:
The authors do not have any competing financial interest to declare.

Acknowledgements

This project was supported by The Scientific and Technological Research Council of Turkey (TUBITAK- Grant No 118S398).

Appendix A. Supplementary data

Supplementary data to this article can be found online at https://doi.org/10.1016/j.cbi.2024.111303.

Data availability

Data will be made available on request.

References

[1] Y. Khan, et al., Classification, synthetic, and characterization approaches to nanoparticles, and their applications in various fields of nanotechnology: a review, Catalysts 12 (11) (Nov. 2022) 1386, https://doi.org/10.3390/catal12111386.
[2] G. Bystrzejewska-Piotrowska, J. Golimowski, P.L. Urban, Nanoparticles: their potential toxicity, waste and environmental management, Waste Manag. 29 (9) (Sep. 2009) 2587–2595, https://doi.org/10.1016/j.wasman.2009.04.001.
[3] I. Khan, K. Saeed, I. Khan, Nanoparticles: properties, applications and toxicities, Arab. J. Chem. 12 (7) (Nov. 2019) 908–931, https://doi.org/10.1016/j.arabjc.2017.05.011.
[4] M. De, P.S. Ghosh, V.M. Rotello, Applications of nanoparticles in biology, Adv. Mater. 20 (22) (2008) 4225–4241, https://doi.org/10.1002/adma.200703183.
[5] A. López-Serrano, R.M. Olivas, J.S. Landaluze, C. Cámara, Nanoparticles: a global vision. Characterization, separation, and quantification methods. Potential environmental and health impact, Anal. Methods 6 (1) (Dec. 2013) 38–56, https://doi.org/10.1039/C3AY40517F.
[6] B. Saltepe, E.U. Bozkurt, N. Hacıosmanoğlu, U.Ö.Ş. Şeker, Genetic circuits to detect nanomaterial triggered toxicity through engineered heat shock response mechanism, ACS Synth. Biol. 8 (10) (Oct. 2019) 2404–2417, https://doi.org/10.1021/acssynbio.9b00291.
[7] A. Seaton, L. Tran, R. Aitken, K. Donaldson, Nanoparticles, human health hazard and regulation, J. R. Soc., Interface 7 (Suppl 1) (Feb. 2010) S119–S129, https://doi.org/10.1098/rsif.2009.0252.focus. Suppl 1.
[8] S. Anthérieu, C. Chesné, R. Li, C. Guguen-Guillouzo, A. Guillouzo, Optimization of the HepaRG cell model for drug metabolism and toxicity studies, Toxicol. Vitro 26 (8) (Dec. 2012) 1278–1285, https://doi.org/10.1016/j.tiv.2012.05.008.
[9] M.-J. Marion, O. Hantz, D. Durantel, The HepaRG cell line: biological properties and relevance as a tool for cell biology, drug metabolism, and virology studies, in: P. Maurel (Ed.), Hepatocytes: Methods and Protocols, Methods in Molecular Biology, Humana Press, Totowa, NJ, 2010, pp. 261–272, https://doi.org/10.1007/978-1-60761-688-7_13.
[10] S. Gunti, A.T.K. Hoke, K.P. Vu, N.R. London, Organoid and spheroid tumor models: techniques and applications, Cancers 13 (4) (Jan. 2021) 874, https://doi.org/10.3390/cancers13040874.
[11] S.J. Fey, K. Wrzesinski, Determination of drug toxicity using 3D spheroids constructed from an immortal human hepatocyte cell line, Toxicol. Sci. 127 (2) (Jun. 2012) 403–411, https://doi.org/10.1093/toxsci/kfs122.
[12] H. Tseng, et al., A spheroid toxicity assay using magnetic 3D bioprinting and real-time mobile device-based imaging, Sci. Rep. 5 (1) (Sep. 2015) 13987, https://doi.org/10.1038/srep13987.
[13] E. Flampouri, S. Imar, K. Oconnell, B. Singh, Spheroid-3D and monolayer-2D intestinal electrochemical biosensor for toxicity/viability testing: applications in drug screening, food safety, and environmental pollutant analysis, ACS Sens. 4 (3) (Mar. 2019) 660–669, https://doi.org/10.1021/acssensors.8b01490.
[14] N. Celebi, M.Y. Aydin, F. Soysal, Y.O. Ciftci, K. Salimi, Ligand-free fabrication of Au/TiO2 nanostructures for plasmonic hot-electron-driven photocatalysis: photoelectrochemical water splitting and organic-dye degredation, J. Alloys Compd. 860 (Jan) (2021), https://doi.org/10.1016/j.jallcom.2020.157908.
[15] N. Celebi, Bio-inspired NIR responsive Au-pDA@pDA sandwich nanostructures with excellent photo-thermal performance and stability, Colloids Surf. A Physicochem. Eng. Asp. 611 (Jan. 2021) 125758 [Online]. Available: https://www.academia.edu/98225702/Bio_inspired_NIR_responsive_Au_pDA_at_pDA_sandwich_nanostructures_with_excellent_photo_thermal_performance_and_stability. (Accessed 8 July 2024).
[16] D.D. Usta, K. Salimi, A. Pinar, İ. Coban, T. Tekinay, A. Tuncel, A boronate affinity-assisted SERS tag equipped with a sandwich system for detection of glycated hemoglobin in the hemolysate of human erythrocytes, ACS Appl. Mater. Interfaces 8 (19) (May 2016) 11934–11944, https://doi.org/10.1021/acsami.6b00138.
[17] N. Celebi, F. Soysal, K. Salimi, Spherical shape-defined hollow UiO-66 metal-organic frameworks with superior incident photon scattering for enhanced photoelectrochemical H-2 evolution, J. Colloid Interface Sci. 608 (Jan. 2022) 1238–1246, https://doi.org/10.1016/j.jcis.2021.10.145.
[18] Mussel-inspired polydopamine coating as a versatile platform for synthesizing polystyrene/Ag nanocomposite particles with enhanced antibacterial activities" - Journal of Materials Chemistry B (RSC Publishing). Accessed: July. 8, 2024. [Online]. Available: https://pubs.rsc.org/en/content/articlelanding/2014/tb/c4tb00460d.
[19] M. Pertea, D. Kim, G.M. Pertea, J.T. Leek, S.L. Salzberg, Transcript-level expression analysis of RNA-seq experiments with HISAT, StringTie and Ballgown, Nat. Protoc. 11 (9) (Sep. 2016), https://doi.org/10.1038/nprot.2016.095. Art. no. 9.
[20] Spheroid-based drug screen: considerations and practical approach, Nat. Protoc. 4, 309–324. [Online]. Available: https://www.nature.com/articles/nprot.2008.226. (Accessed 25 September 2024).
[21] K. Zhang, et al., A novel function of IMPA2, plays a tumor-promoting role in cervical cancer, Cell Death Dis. 11 (5) (May 2020) 1–14, https://doi.org/10.1038/s41419-020-2507-z.
[22] X. Lei, et al., IMPA2 promotes basal-like breast cancer aggressiveness by a MYC-mediated positive feedback loop, Cancer Lett. 582 (Feb. 2024) 216527, https://doi.org/10.1016/j.canlet.2023.216527.
[23] Y. Tian, Q. Luo, K. Huang, T. Sun, S. Luo, Long noncoding RNA AC078850.1 induces NLRP3 inflammasome-mediated pyroptosis in atherosclerosis by upregulating ITGB2 transcription via transcription factor HIF-1α, Biomedicines 11 (6) (Jun. 2023) 1734, https://doi.org/10.3390/biomedicines11061734.
[24] Expression of OPN3 in lung adenocarcinoma promotes epithelial-mesenchymal transition and tumor metastasis - xu, in: Thoracic Cancer, Wiley Online Library, 2020. https://onlinelibrary.wiley.com/doi/10.1111/1759-7714.13254. (Accessed 19 October 2023).
[25] Z. Zhang, H. Jiang, Y. Wang, M. Shi, Heparan sulfate D-glucosamine 3-O-sulfotransferase 3B1 is a novel regulator of transforming growth factor-beta-mediated epithelial-to-mesenchymal transition and regulated by miR-218 in nonsmall cell lung cancer, J. Cancer Res. Therapeut. 14 (1) (Jan. 2018) 24–29, https://doi.org/10.4103/jcrt.JCRT_659_17.
[26] K. Song, Q. Li, Z.-Z. Jiang, C.-W. Guo, P. Li, Heparan sulfate D-glucosaminyl 3-O-sulfotransferase-3B1, a novel epithelial-mesenchymal transition inducer in pancreatic cancer, Cancer Biol. Ther. 12 (5) (Sep. 2011) 388–398, https://doi.org/10.4161/cbt.12.5.15957.
[27] Y.-C. Wu, et al., NUP85 alleviates lipid metabolism and inflammation by regulating PI3K/AKT signaling pathway in nonalcoholic fatty liver disease, Int. J. Biol. Sci. 20 (6) (2024) 2219–2235, https://doi.org/10.7150/ijbs.92337.
[28] S.P. Rendic, Metabolism and interactions of Ivermectin with human cytochrome P450 enzymes and drug transporters, possible adverse and toxic effects, Arch. Toxicol. 95 (5) (May 2021) 1535–1546, https://doi.org/10.1007/s00204-021-03025-z.
[29] M. Zhao, et al., Cytochrome P450 enzymes and drug metabolism in humans, Int. J. Mol. Sci. 22 (23) (Nov. 2021) 12808, https://doi.org/10.3390/ijms222312808.
[30] M. Ingelman-Sundberg, Human drug metabolising cytochrome P450 enzymes: properties and polymorphisms, Naunyn-Schmiedeberg's Arch. Pharmacol. 369 (1) (Jan. 2004) 89–104, https://doi.org/10.1007/s00210-003-0819-z.
[31] E. Girardi, et al., A widespread role for SLC transmembrane transporters in resistance to cytotoxic drugs, Nat. Chem. Biol. 16 (4) (Apr. 2020) 469–478, https://doi.org/10.1038/s41589-020-0483-3.
[32] B. Ruttkay-Nedecky, et al., The role of metallothionein in oxidative stress, Int. J. Mol. Sci. 14 (3) (Mar. 2013), https://doi.org/10.3390/ijms14036044, 3.
[33] H. Ma, et al., The metal ion release of manganese ferrite nanoparticles: kinetics, effects on magnetic resonance relaxivities, and toxicity, ACS Appl. Bio Mater. 5 (6) (Jun. 2022) 3067–3074, https://doi.org/10.1021/acsabm.2c00338.
[34] T. Kamiya, K. Takeuchi, S. Fukudome, H. Hara, T. Adachi, Copper chaperone antioxidant-1, Atox-1, is involved in the induction of SOD3 in THP-1 cells, Biometals 31 (1) (Feb. 2018) 61–68, https://doi.org/10.1007/s10534-017-0067-1.
[35] D.-D. Ma, W.-X. Yang, Engineered nanoparticles induce cell apoptosis: potential for cancer therapy, Oncotarget 7 (26) (Apr. 2016) 40882–40903, https://doi.org/10.18632/oncotarget.8553.
[36] F. Wang, et al., Silver nanoparticles induce apoptosis in HepG2 cells through particle-specific effects on mitochondria, Environ. Sci. Technol. 56 (9) (May 2022) 5706–5713, https://doi.org/10.1021/acs.est.1c08246.
[37] S.N. Hart, Y. Li, K. Nakamoto, E. Subileau, D. Steen, X. Zhong, A comparison of whole genome gene expression profiles of HepaRG cells and HepG2 cells to primary human hepatocytes and human liver tissues, Drug Metab. Dispos. 38 (6) (Jun. 2010) 988–994, https://doi.org/10.1124/dmd.109.031831.
[38] Three-dimensional HepaRG spheroids as a liver model to study human genotoxicity in vitro with the single cell gel electrophoresis assay Sci. Rep. 9 (September 2024) 10548 [Online]. Available: https://www.nature.com/articles/s41598-019-47114-7.

[39] P. Xiong, et al., Cytotoxicity of metal-based nanoparticles: from mechanisms and methods of evaluation to pathological manifestations, Adv. Sci. 9 (16) (2022) 2106049, https://doi.org/10.1002/advs.202106049.
[40] G. Xu, et al., Upregulated expression of MMP family genes is associated with poor survival in patients with esophageal squamous cell carcinoma via regulation of proliferation and epithelial-mesenchymal transition, Oncol. Rep. 44 (1) (Jul. 2020) 29–42, https://doi.org/10.3892/or.2020.7606.
[41] X.-L. Chen, Y.-M. Xu, A.T.Y. Lau, Toxic metals in the regulation of epithelial–mesenchymal plasticity: demons or angels? Cancer Cell Int. 22 (1) (Jul. 2022) 237, https://doi.org/10.1186/s12935-022-02638-3.
[42] A. Nel, T. Xia, L. Mädler, N. Li, Toxic potential of materials at the nanolevel, Science 311 (5761) (Feb. 2006) 622–627, https://doi.org/10.1126/science.1114397.
[43] R. Santacruz-Márquez, J.A. Flaws, L. del C. Sánchez-Peña, I. Hernández-Ochoa, Exposure to zinc oxide nanoparticles increases estradiol levels and induces an antioxidant response in antral ovarian follicles in vitro, Toxics 11 (7) (Jul. 2023) 602, https://doi.org/10.3390/toxics11070602.
[44] A. Bettiol, et al., Erythrocyte oxidative stress and thrombosis, Expet Rev. Mol. Med. 24 (Aug. 2022) e31, https://doi.org/10.1017/erm.2022.25.
[45] E. Lopez-Huertas, W.L. Charlton, B. Johnson, I.A. Graham, A. Baker, Stress induces peroxisome biogenesis genes, EMBO J. 19 (24) (Dec. 2000) 6770–6777, https://doi.org/10.1093/emboj/19.24.6770.
[46] M. Nordgren, M. Fransen, Peroxisomal metabolism and oxidative stress, Biochimie 98 (Mar. 2014) 56–62, https://doi.org/10.1016/j.biochi.2013.07.026.
[47] R. Wan, Y. Mo, L. Feng, S. Chien, D.J. Tollerud, Q. Zhang, DNA damage caused by metal nanoparticles: the involvement of oxidative stress and activation of ATM, Chem. Res. Toxicol. 25 (7) (Jul. 2012) 1402–1411, https://doi.org/10.1021/tx200513t.
[48] Y. Yao, T. Zhang, M. Tang, The DNA damage potential of quantum dots: toxicity, mechanism and challenge, Environ. Pollut. 317 (Jan. 2023) 120676, https://doi.org/10.1016/j.envpol.2022.120676.
[49] M.R.R. de Planque, S. Aghdaei, T. Roose, H. Morgan, Electrophysiological characterization of membrane disruption by nanoparticles, ACS Nano 5 (5) (May 2011) 3599–3606, https://doi.org/10.1021/nn103320j.
[50] Multi-omics approaches confirm metal ions mediate the main toxicological pathways of metal-bearing nanoparticles in lung epithelial A549 cells - Environmental Science: Nano (RSC Publishing).” Accessed: August. 31, 2023. [Online]. Available: https://pubs.rsc.org/en/content/articlelanding/2018/en/c8en00071a.
[51] A. Manke, L. Wang, Y. Rojanasakul, Mechanisms of nanoparticle-induced oxidative stress and toxicity, BioMed Res. Int. 2013 (2013) 942916, https://doi.org/10.1155/2013/942916.
[52] Z. Yu, et al., Reactive oxygen species-related nanoparticle toxicity in the biomedical field, Nanoscale Res. Lett. 15 (1) (Dec. 2020) 115, https://doi.org/10.1186/s11671-020-03344-7.
[53] A.V. Kozlov, S. Javadov, N. Sommer, Cellular ROS and antioxidants: physiological and pathological role, Antioxidants 13 (5) (May 2024), https://doi.org/10.3390/antiox13050602.
[54] L. He, T. He, S. Farrar, L. Ji, T. Liu, X. Ma, Antioxidants maintain cellular redox homeostasis by elimination of reactive oxygen species, Cell. Physiol. Biochem. 44 (2) (Nov. 2017) 532–553, https://doi.org/10.1159/000485089.
[55] P. Chen, Detection of DNA damage response caused by different forms of titanium dioxide nanoparticles using sensor cells, J. Biosens. Bioelectron. 3 (5) (2012), https://doi.org/10.4172/2155-6210.1000129.
[56] K. Klien, J. Godnić-Cvar, Genotoxicity of metal nanoparticles: focus on in vivo studies, Arh. Hig. Rada. Toksikol. 63 (2) (Jun. 2012) 133–145, https://doi.org/10.2478/10004-1254-63-2012-2213.
[57] M. Ahamed, et al., DNA damage response to different surface chemistry of silver nanoparticles in mammalian cells, Toxicol. Appl. Pharmacol. 233 (3) (Dec. 2008) 404–410, https://doi.org/10.1016/j.taap.2008.09.015.
[58] H.K. Lim, P.V. AshaRani, M.P. Hande, Enhanced genotoxicity of silver nanoparticles in DNA repair deficient mammalian cells, Front. Genet. 3 (2012) [Online]. Available: https://www.frontiersin.org/articles/10.3389/fgene.2012.00104. (Accessed 19 October 2023).
[59] H. Yeo, H. Lee, S.-M. Park, H.N. Kang, Paeoniae radix overcomes resistance to EGFR-TKIs via aurora B pathway suppression in lung adenocarcinoma, Life Sci. 357 (Nov. 2024) 123097, https://doi.org/10.1016/j.lfs.2024.123097.
[60] H. Wang, M. Guo, H. Wei, Y. Chen, Targeting p53 pathways: mechanisms, structures and advances in therapy, Signal Transduct. Targeted Ther. 8 (1) (Mar. 2023) 1–35, https://doi.org/10.1038/s41392-023-01347-1.
[61] Y.-J. Guo, W.-W. Pan, S.-B. Liu, Z.-F. Shen, Y. Xu, L.-L. Hu, ERK/MAPK signalling pathway and tumorigenesis, Exp. Ther. Med. 19 (3) (Mar. 2020) 1997–2007, https://doi.org/10.3892/etm.2020.8454.
[62] M. Laplante, D.M. Sabatini, mTOR signaling at a glance, J. Cell Sci. 122 (20) (Oct. 2009) 3589–3594, https://doi.org/10.1242/jcs.051011.